

CHAPTER 14

MACRO-TURBULENCE FROM WIND WAVES

Chun-Yuan Lee¹ and Frank D. Masch²

ABSTRACT

Laboratory studies in a wind wave flume were carried out to investigate the macro-scale turbulence associated with wind waves and white cap conditions. Velocity fluctuations in water were measured with a hot film anemometer and parametric correlations between wind waves and turbulence characteristics were established. Measured data were recorded in analog form, digitized and stored on magnetic tape. Auto-covariance functions and power spectral density functions were then obtained for all sample records.

Results showed that the depth of the penetration of the macro-scale turbulence increased rapidly with wind speed but the rate of penetration diminished at the higher wind speeds. This rate of macro-turbulence penetration was found to vary inversely with wave height and wave steepness. Most turbulent fluctuations having frequencies equal to or higher than the frequency of the ambient surface waves were confined to the zone of macro-turbulence penetration although some disturbances such as vortex rings and other turbulence associated with white cap wave conditions occasionally penetrated to greater depths. It was found that the energy dissipation increased with wave height and that almost all wave energy dissipation was concentrated near the water surface.

INTRODUCTION

Turbulence has been analyzed and described variously in terms of instantaneous velocity fluctuations, correlation functions, power spectral density functions, eddy viscosity, mixing length, and turbulent shear stress. Yet, much of the experimental work on fluid turbulence has been on the relatively special cases of steady flow or plane Couette flow. Most of this experimentation has been largely conducted in wind tunnels, pipes and conduits. Very little experimentation has been on the "basics" of the phenomenon of macro-turbulence created by wind induced waves.

The objectives of this investigation are (1) To obtain some insight into the phenomenon of macro-turbulence in large natural bodies of water due to wind induced waves and (2) To establish empirical parametric correlations between the major interrelated elements of the macro-turbulence phenomenon. Underlying this investigation is the requirement to seek feasible practical solutions to the subsidiary objectives of pollution control based on the efficient use of the natural mixing and dispersion processes in natural bodies of water.

¹ Assistant Professor of Civil Engineering, Tri-State College, Angola, Indiana

² Special Consultant for Fischlin, Zurich, Switzerland and Austin (on leave from The University of Texas at Austin)

Energy from wind is imparted to water through shear stress at the interface, the "sheltering effect" on the lee side of individual waves, or the action of turbulent pressure fluctuations of the air stream. Some of the energy is absorbed in the form of a thin surface layer of flow called wind drift. Some energy is dissipated through viscosity in orbital motions of water particles. Additional dissipation occurs when surface drift interacts with orbital motions and wave breaking. As the wind grows stronger and the waves approach fully developed conditions, energy dissipation continues to increase until an equilibrium state is reached with respect to energy input from the wind. It appears that the increased energy dissipation results mostly from intensified interaction between the wind, wind drift, wave breaking, and orbital motion of water particles. Since these are mainly surface phenomena, it can be inferred that the macro-scale turbulence induced by wind waves is highly anisotropic. Thus, auto-correlation and power spectrum functions appear to be the most viable means of analysis. Furthermore, since the diffusive action of turbulence is believed to be determined mainly by the larger eddies, primary emphasis is placed on the lower frequency portion of the power spectrum.

Systematic measurements in a wind wave flume gave sample records of surface waves and velocity fluctuations for various combinations of water depths and wind speeds. Assuming random Gaussian processes, each sample record was regarded as representative of the entire ensemble. Comparisons of auto-correlation functions of surface waves and those of velocity fluctuations permitted evaluation of an arbitrarily defined depth of penetration of macro-turbulence. Relative intensity of turbulence at different depths from the surface can also be inferred from power spectrum functions. This information permits a more realistic assessment of the effects of wind and waves on the mixing and dispersion processes in natural bodies of water.

EXPERIMENTAL APPARATUS AND TEST PROCEDURES

Experimental Apparatus

All experiments were carried out in a 70 ft wind wave flume at The University of Texas at Austin. This flume is 11 ft wide, 2-1/2 ft deep, and is equipped with a 4500 cfm blower. The blower is attached so that air is drawn in at the upwind end of the closed flume through a vaned intake and then discharged through the blower to the atmosphere at the downwind end of the flume. The wind velocity was controlled by a vane installed at the throat section in the flume near the blower. This arrangement had the advantages that wind speed inside the flume could be effectively reduced without causing large pressure drops in the flume, and by leaving the entrance unobstructed, the streamlined guide vane produced relatively uniform inflow of the wind at all wind speeds. Wind velocities up to 40 fps were obtainable in the flume and were measured with a standard Prandtl-type pitot tube connected to a Uehling Type-B inclined draft gage. Wave absorbers were installed at the end of the flume to help dampen out oscillations and reduce reflections.

Continuous records of the heights and periods of the wind generated waves were measured with parallel wire wave gages inserted through the top cover of the flume. The outputs from the wave gages were recorded on a two channel oscillograph equipped with carrier preamplifiers.

To measure velocity fluctuations in fluids, many approaches have been tried. Macovsky [1] found that impurities in water prevented stable operation of hot-wire anemometers. Beginning in 1949 studies were undertaken at MIT to develop an instrument for turbulence measurements in water which would be free from the troubles encountered by hot-wires. This effort resulted in an impact tube-pressure cell combination, Ippen, et al [2] which measured the fluctuation in dynamic head at the tip of the impact tube by means of the change in electrical capacitance between a diaphragm and a fixed electrode. However any device based on this principle has relatively low natural frequency, picks up static pressure fluctuations as well as the dynamic head associated with the velocity fluctuations and is suited best for measurements of low intensity turbulence. Lumley [3] reported the use of a hot-thermistor probe for measuring turbulence. The main disadvantage of this device is the difficulty in attaining high frequency response.

The measurements involved in this study were made with the Heat Flux System Model 1010 constant temperature hot-film anemometer. This instrument consists basically of a power supply, wheatstone bridge, feedback amplifier, and readout meter. The bridge has two fixed resistance legs, a cylindrical sensor, and a three stage resistance decade. The frequency response reported by the manufacturer ranges from 0 cps to 1,000 cps.

The cylindrical hot-film sensor consists of a pyrex glass rod coated with a thin platinum film and sputtered with a thin layer of quartz. The platinum and quartz coatings are each approximately 10^{-5} inches in thickness. The quartz coating reduces bubble formation and electrical shunts across the sensor. This helps to eliminate the requirement for pure water and greatly reduces the effect of contamination of the surface. The sensor used in this study was 0.002 inches in diameter and 0.040 inches long.

In order to obtain a good calibration, an effort was made to assure the kinematical resemblance between the conditions of operation and calibration. Since a fixed sensor inserted into a water body under wave action experiences a periodic flow that changes direction continually each cycle a special calibration unit was built. This unit consisted of a half-horsepower electrical motor and a Vickers transmission and gear combination that supported an aluminum rod which held the sensor holder in a vertical position while undergoing an "irrotational rotation". This resulted in a periodic circular motion of the sensor relative to the still water. The amplitude of the circular motion could be adjusted by varying the position of the supporting points. Prior to a series of measurements analog wave records were obtained and samples of wave heights were chosen at random intervals and plotted against the corresponding wave periods. After about 30 waves had been obtained and plotted in this way a distance equal to the model wave amplitudes was taken as the distance from the axis of the wheel to the supporting points of the aluminum rod. This corresponded to the amplitude of the circular motion for the sensor. During calibration, the rotating speed of the wheel was first maintained constant long enough for the angular speed to be measured and for the output from the hot-film anemometer to be observed and recorded. As some effect of the supporting rod vibration was present during calibration, the average value of the output was assumed to represent the true sensor velocity. A second speed was then maintained and recorded as before. Repetition of this process before each series of velocity fluctuation measurements enabled the determination of the mean velocity experienced by the sensor under various wave actions.

The sensor stand was placed 60 feet from the entrance section of the flume. This location provided a long fetch yet remained some distance from the downwind end of the flume. During actual operations two external sources contributed to the vibration of the sensor, and gave signals irrelevant to the velocity fluctuations. The first was the vibration of the flume due to the blower and motor. The second was the vibration of the support rod for the sensor unit caused by the drag of the wind and waves in the flume. The following measures were taken to reduce the vibration of the sensor. First, the sensor stand was built of steel channels solidly welded together and was used to support the sensor independently of the flume. Secondly, the support rod was firmly attached to the sensor stand inserted through a hole in the top cover of the flume, and fastened with a very thin wire at the lower end near the sensor to dampen out vibrations. Finally the throat section connecting the flume and the blower was cut and re-sealed by masking tape to practically eliminate the transmission of vibration from the blower to the flume.

Water in the flume was kept clean by regular replacement. Before any measurements were taken with the hot-film sensor, new water was allowed to stand in the flume at least 24 hours to reduce the air content of the water and thus, the chance of bubble formation at the surface of the sensor which tended to create hot spots on the sensor surface and cause "erosion" of the quartz coating. If the quartz coating is deteriorating the cold resistance of the sensor drifts and no meaningful measurements are possible. Under such conditions the sensor soon fails completely.

Test Procedures

All experiments associated with the present study were designed in such a way that the characteristics and relative intensities of wind wave turbulence at various distances below the still water surface could be compared with one another under statistically constant wave conditions. In order to attain this objective, the water depth in the wave flume was first set at a predetermined level, a constant wind speed was maintained and the sensor was inserted into the water to measure the velocity fluctuations at a fixed point below the actual water surface, and a sample record was measured. The elevation of the sensor was then changed successively until sample records were obtained for a number of points uniformly spaced over the depth. Usually the spacing was taken to be 0.1 foot and the uppermost point was about 0.05 to 0.1 foot below the still water level, depending upon the wave conditions. This constituted one series of sample records from which information could be derived and the lower limit of penetration of the macro-scale turbulence associated with the wind waves estimated. The wind speed was then varied and the experiment repeated. Finally, the water depth was also varied to provide new wave conditions under different wind speeds.

Theoretically, sample record should be as long in real time as possible but there are several limitations to this requirement. To avoid the appearance of a squeezed or even blurred trace and to minimize human error in the digitizing process widely spaced records are desirable. These considerations favor a higher chart speed which means a shorter sample record in real time for a constant length of strip chart. Since the dimensions of the digitizing machine (the Pencil Follower) limited the effective chart length to about three feet (90 cm) a chart speed of 20 mm/sec was selected for all measurements. This chart speed and resulting chart length represented an actual operation time of 45 seconds and covered from 90 to 150 waves. When digitized, from 1800 to 3000 discrete points were obtained to describe the original sample record.

ANALYSIS OF RESULTS

Basic Data

Measurements of surface waves and velocity fluctuations were made at water depths of 0.7, 1.0 and 1.2 ft respectively. Three different wind speeds were applied successively at each water depth resulting in three series of measurements reflecting the variations of water particle velocity fluctuations at different depths. A total of 96 sample records were obtained. Wind velocity profiles at the center of the flume and contour lines of wind velocity in a cross-section were also obtained. Generally speaking, the wind velocity distributions in the wave flume were relatively uniform and the maximum cross-sectional velocity ranged from 13 to 40 fps with the corresponding Reynolds number varying from 2.44×10^4 to 7.51×10^4 .

Mathematical Considerations

It is desirable at this point to make a summary analysis of the variables and the relations involved in the application of the stochastic process model approach adopted for this study. There are many useful expositions and interpretations of the mathematical rationale underlying such methods in standard texts on stochastic methods, noise theory and random process analysis [4, 5, 6].

Suppose a stationary random process $y(t)$ has been given in the form of a time history record. The mean value μ is

$$\mu = \lim_{T \rightarrow \infty} \frac{1}{T} \int_0^T y(t) dt \quad (1)$$

where T is the length of the record. The mean square value ψ^2 is

$$\psi^2 = \lim_{T \rightarrow \infty} \frac{1}{T} \int_0^T y^2(t) dt \quad (2)$$

and the positive square root of this value is called the root mean square or rms value. The variance, σ^2 , is

$$\sigma^2 = \lim_{T \rightarrow \infty} \int_0^T [y(t) - \mu]^2 dt \quad (3)$$

The positive square root of the variance is called the standard deviation. By expanding Eq. (3), it can be shown that

$$\mu^2 = \sigma^2 + \psi^2 \quad (4)$$

The auto-covariance function $C(\tau)$ is defined as

$$C(\tau) = \lim_{T \rightarrow \infty} \frac{1}{T} \int_{-T/2}^{T/2} y(t) y(t + \tau) dt \quad (5)$$

when the mean value of μ of the process is assumed to be zero. When $\mu \neq 0$

$$C(\tau) = \lim_{T \rightarrow \infty} \frac{1}{T} \int_{-T/2}^{T/2} [y(t) - \mu] [y(t + \tau) - \mu] dt \quad (6)$$

In Eqs (5) and (6) τ represents a time lag. $C(\tau)$ is also frequently called the "autocorrelation function" although this term should be applied to the normalized ratio $C(\tau)/C(0)$.

The power spectral density function $P(f)$ may be defined as

$$P(f) = \int_{-\infty}^{\infty} C(\tau) e^{-i2\pi f\tau} d\tau \quad (7)$$

where f is the frequency of the fluctuation of the process at a certain point in the frequency domain and $i = \sqrt{-1}$. It can be seen that $P(f)$ and $C(\tau)$ are Fourier transforms of each other. From the stationary hypothesis the auto-covariance function is an even function of τ , and from Eqs (5) and (6), it can be seen that $C(\tau)$ is a real function. Thus,

$$\begin{aligned} C(\tau) &= \int_{-\infty}^{\infty} P(f) e^{i2\pi f\tau} df \\ &= \int_{-\infty}^{\infty} P(f) \cos 2\pi f\tau df + i \int_{-\infty}^{\infty} P(f) \sin 2\pi f\tau df \\ &= \int_{-\infty}^{\infty} P(f) \cos 2\pi f\tau df = \text{real function} \end{aligned} \quad (8)$$

By inverse transformation or a similar argument

$$P(f) = \int_{-\infty}^{\infty} C(\tau) \cos 2\pi f\tau d\tau \quad (9)$$

Since $C(\tau)$ is an even function $P(f)$ should also be even. The above relations for the real valued two-sided power spectral density function $P(f)$ may be simplified to

$$P(f) = 2 \int_0^{\infty} C(\tau) \cos 2\pi f\tau d\tau \quad (10)$$

The physically realizable one-sided power spectral density function $V(f)$ is defined by

$$V(f) = 2 P(f) = 4 \int_0^{\infty} C(\tau) \cos 2\pi f\tau d\tau \quad (11)$$

$0 \leq f < \infty$

For practical applications, the record lengths are limited and the y values involved in the actual calculations are uniformly distributed along the time axis. Discrete forms of the above equations for numerical calculations, are given as follows

$$\mu \approx \bar{y} = \frac{1}{N} \sum_{I=1}^N y(I) \tag{12}$$

where N is the total number of data points. The auto-covariance C_M is given by

$$C_M = \frac{1}{N - M + 1} \sum_{I=1}^{N - M + 1} y(I) y(I + M - 1) \tag{13}$$

where $l = 1, 2, 3$, N and $M = 1, 2, 3$. Ml . In this study Ml is assumed to be $N/10$. The lag time $\tau = (M-1)\Delta t$ for a data sampling interval Δt .

The power spectral density function $V(f)$ is calculated from

$$V_J = \text{one-sided power spectral density function} \\ = 2\Delta t \left\{ C_1 + 2 \sum_{K=2}^{Ml-1} C_k \cos [(K-1)(J-1)\pi/(Ml-1)] + C_{Ml} \cos [(J-1)\pi] \right\} \tag{14}$$

where $J = 1, 2, 3$, Ml . This is an estimate of the power spectrum associated with the discrete covariance function defined by Eq. (13) rather than the continuous function of Eq. (16). For this discrete cosine transformation the spectral estimates at any frequency are affected by the energy in neighboring frequencies. It is apparent, therefore, that a smoothing operation is desirable. In this study, the Hanning procedure, [7], was performed on the above raw spectrum V_J , to obtain the so-called refined spectrum U

$$U_1 = 0.5V_1 + 0.5V_2 \\ U_{Ml} = 0.5V_{Ml-1} + 0.5V_{Ml} \\ U_l = V_l + 0.5(V_{l-1} + V_{l+1}) \tag{15}$$

where $l = 2, 3, 4, \dots, (Ml - 1)$. Note that in order to facilitate computer programming, the notation is such that U_1 stands for $C(0)$, U_2 for $C(\Delta t)$, U_l for $C[(l-1)\Delta t]$, etc. Eqs. (12), (13), (14) and (15) form the basis for the numerical evaluation of the auto-covariance and power spectral density function.

Digitizing and Computing Procedures

To digitize the sample records, each paper chart was placed on a 51" x 54" table with a magnetic field below the surface. The curve on the chart was traced with a special "pencil" which responded to the magnetic field and identified its position in terms of x- and y-values in arbitrary but predetermined units. These digitized values as well as calibration and identification data were stored on a magnetic tape through an incremental

tape recorder. By means of a high speed digital computer, the raw data were decoded and transformed into grid point data uniformly spaced on the time axis using a straight-line fit. Wave characteristics, auto-covariance and power spectral functions were calculated and then tabulated and plotted on microfilm.

Interpretation of Results

A random process may be classified as wide-banded if it consists of fluctuations of various frequencies, narrow banded if the range of frequencies is limited. The auto-covariance function of a wide-band random process diminishes rapidly as the lag time is increased, for a narrow-band random process the diminishing rate is slow [1]. Inspection of the auto-covariance plots for each test series (Fig. 1 is illustrative of a typical test series) revealed that the surface wave fluctuations appeared as narrow-band random processes and velocity fluctuations appeared as wide-band random processes near the water surface and narrow-banded at greater depths. Thus the spatial pattern of transition of the velocity records from one type of fluctuation to the other gives an estimate of the depth of penetration of wind-wave induced macro-turbulence.

For each power spectral plot of surface wave record (Fig. 2 is typical) there is only one major peak which always centers around the frequency corresponding to the mean wave period which, for this study, varied from about 0.38 to 0.63 seconds. For velocity fluctuations measured near the water surface, there is also a major peak centering around the frequency of the mean surface wave, but the smaller peaks at higher frequencies are relatively significant. However, for velocity fluctuations measured at a considerable distance below the surface, the trend is again toward the dominance of a major peak centering around the frequency of the mean surface wave.

The power spectral density function for random data describes the general frequency composition of the data in terms of the spectral density of its mean square value. Integration of the power spectral density function between two frequency values represents the amount contributed to the mean square value by the power spectrum within these limits. Comparison of all the power spectra for a given series of experiments (i.e., for a given combination of water depth and wind speed) permitted the determination of the common lower and upper frequency limits for the first major peak at the mean surface wave frequency. Integration of the power spectrum between these two limits was designated by A_1 . Beyond the upper limit of A_1 the power spectrum decreased in magnitude rather rapidly until a point was reached beyond which it began to flatten out. The change in the slope of the power spectrum was generally somewhere around 8 cps. A common frequency value of this turning point for each series of experiments was also determined from the power spectrum. Integration of the power spectrum between the upper limit of A_1 and this point was designated as A_2 . It was assumed that A_1 essentially represents the contribution from wave motion to the mean square value while A_2 represents the contributions from macro-scale turbulent motions. Although turbulent motions of larger scale comparable to wave motions supposedly were compounded into A_1 , the effect was assumed insignificant and the ratio of A_1 to A_2 was regarded as an indicator of the relative strengths between wave motion and wind wave induced turbulence. In other words, a small A_1/A_2 ratio implies a high turbulent intensity due to wind waves.

Results

Relying mainly on the spatial variation of auto-covariance the depth of penetration of macro-turbulence was estimated for each combination of wind speed and water depth. These data are plotted in Figs 3 through 6. Figure 3 shows that the depth of penetration increases rapidly with maximum wind speed in the flume when the wind speed is relatively low, but the rate of increase diminishes rapidly at higher wind speeds. The maximum wind speed was taken from wind velocity profiles at 0.3 to 0.4 feet above the still water level. In Fig 4, it is seen that when the wave height is small, the depth of penetration increases rapidly with wave height but as the wave height is increased, resistance to increase in depth of penetration becomes stronger. In Fig 5, the ratio, $H_1/10/T^2_{1/10}$, which is proportional to wave steepness using the one-tenth wave height and the corresponding wave period is plotted against depth of penetration. At small steepnesses the penetration increases rapidly, but for the steeper waves, there appears to be a lower limit to the penetration. Since the wave speed c is proportional to the wave period T , $U^2/T^2_{1/10}$ is related to the wave age c/U , where U is the wind speed. Using the same maximum wind speed as in Fig 3, Fig 6 indicates that the depth of penetration correlates quite well with wave age.

Values of A_1/A_2 also were plotted against water depths. Figure 7 is typical of these plots. It is clear that the relative turbulent intensity is much higher near the water surface than below. This tendency is much more evident with lower wind speed than with high wind speed. On the other hand the overall relative intensity of turbulence is much higher for high wind speed (CS 10V01 series) where the return flow is stronger than for low wind speed (e.g. CS 10V04).

For the surface waves, a small A_1/A_2 ratio means widening of the frequency band or a confused sea surface condition. It was interesting to note that the ratio A_1/A_2 correlated quite well with the wave steepness in a way which suggests that the white cap wave condition and consequently the turbulence level in a wind wave system grow in accordance with the characteristic wave steepness.

SUMMARY AND CONCLUSIONS

It is well known that larger eddies generate smaller eddies through inertial interaction thereby transferring energy to the smaller eddies which consume most of the kinetic energy of turbulence through viscous dissipation. However, Von Karman and Lin [7] assumed that the eddy diffusivity might be regarded as a parameter determining the character of the turbulence in the lower-wave number range. In other words the diffusive action of turbulence is determined mainly by the larger eddies. Hence, it can be expected that once the behavior of the macro-turbulence is understood, the relative intensity and spatial distribution of the smaller energy-dissipating eddies could be inferred. This point is reinforced by the tendency for confinement of macro-turbulence to a surface layer a few wave heights in thickness and the existence of high relative turbulent intensity near the water surface. This confirms the finding of Stewart and Grant [8] who based on a study of energy-dissipating eddies concluded that almost all wave dissipation is concentrated near the water surface and decreases rapidly with depth from the surface. Thus rapid and effective mixing near the water surface can be expected in a body of water subject to wind waves.

While direct application of the results of this laboratory study to field situations has to be confirmed by further investigation, the results derived here disclose, qualitatively, the general tendencies under comparable field situations. The main conclusions from this study may be summarized as follows: (1) The depth of the macro-scale turbulence penetration due to the wind induced waves increases rapidly with maximum wind speed but the rate of increase diminishes at higher wind speeds. There is a limiting depth of macro-turbulence penetration which is not exceeded even if the wind velocity is further increased. (2) The rate of increase in the depth of penetration of macro-turbulence varies inversely with wave height, wave length and wave steepness. (3) Most turbulent fluctuations having frequencies higher than the mean frequency of ambient surface waves are confined to the zone of macro-turbulence penetration. This suggests that wind wave induced turbulence is a phenomenon confined essentially to the surface layer with thickness of a few wave heights. However, certain vortex rings or some disturbances associated with white cap wave conditions occasionally penetrate to greater depths, but the elements of the vortex spirals deteriorate into an admixture of random, small scale eddies.

ACKNOWLEDGMENT

This study was supported in part by the Federal Water Quality Administration under Grant 5 RO1 WP00705

REFERENCES

- [1] Macovsky, M S , "The Measurement of Turbulence in Water", Rep No 670, David Taylor Model Basin, Washington, D C , 1948
- [2] Ippen, A T , Tankin, R S , and Raichlen, F , "Turbulence Measurements in Free Surface Flow with an Impact Tube-Pressure Cell Combination", Tech Rep No 20, Hydro Lab, MIT, Cambridge, Mass 1955
- [3] Lumley, J L , "The Constant Temperature Hot-Thermistor Anemometer", Symposium on Measurement in Unsteady Flow ASME, Hydraulics Division Conf Worcester, Mass 1962
- [4] Bendat Julius S , and Piersoll, Allen, G , Measurement and Analysis of Random Data, John Wiley and Sons Inc 1966
- [5] Lee, Y W , Statistical Theory of Communication, John Wiley and Sons, Inc , 1963
- [6] Blackman R B , and Tukey, J W The Measurement of Power Spectra from the Point of View of Communications Engineering, Dover Publications, Inc , 1958
- [7] Karman Th von, and Lin, C C , Advances in Applied Mechanics, 2, 1, 1951
- [8] Stewart, R W , and Grant, H L , "Determination of the Rate of Dissipation of Turbulent Energy Near the Sea Surface in the Presence of Waves", Journal of Geophysical Research, Vol 67, No 8, July, 1962

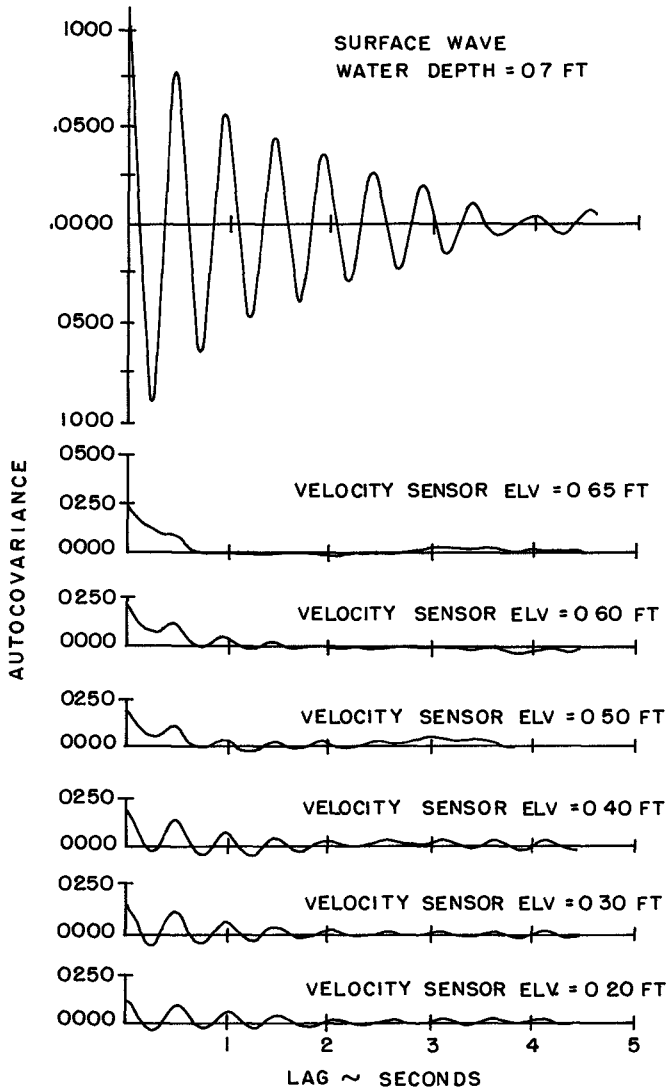


FIG 1 AUTOCOVARANCE VS LAG TIME

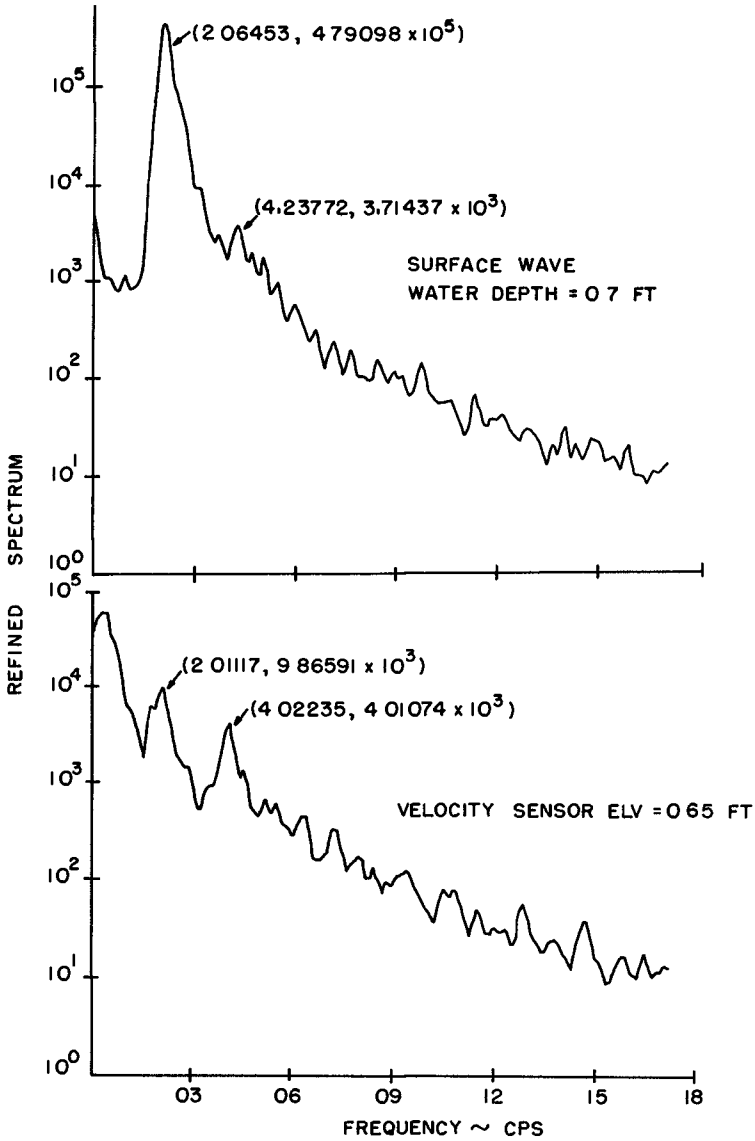


FIG 2A POWER SPECTRAL DENSITY VS FREQUENCY

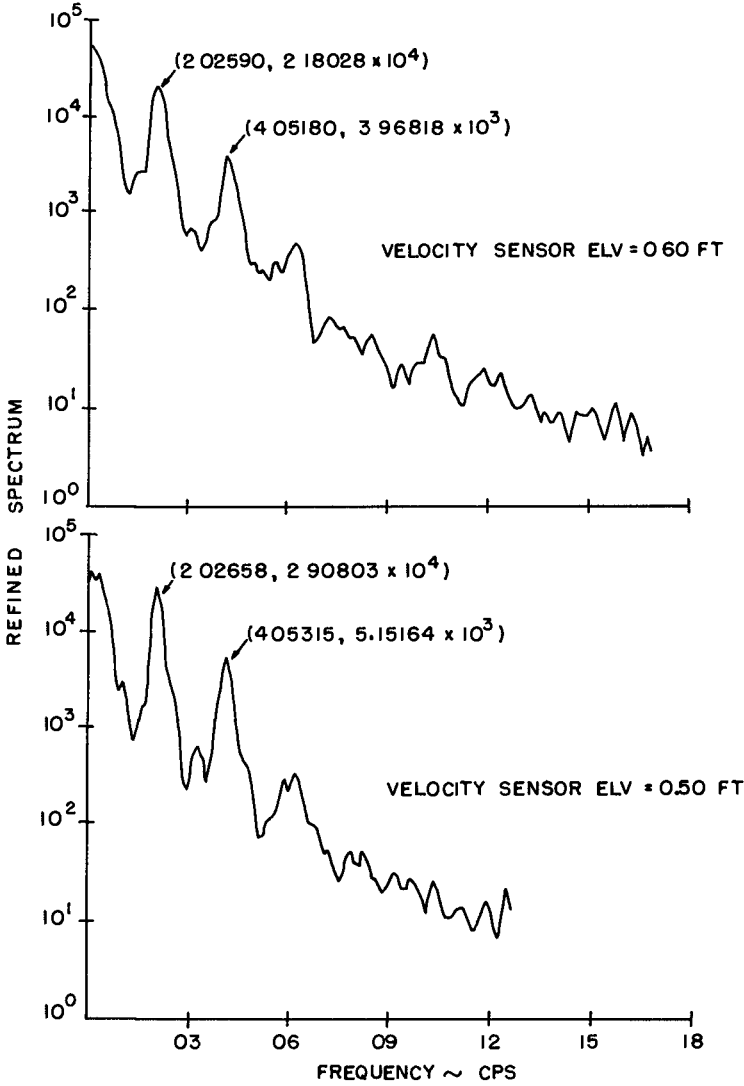


FIG 2B POWER SPECTRAL DENSITY VS FREQUENCY

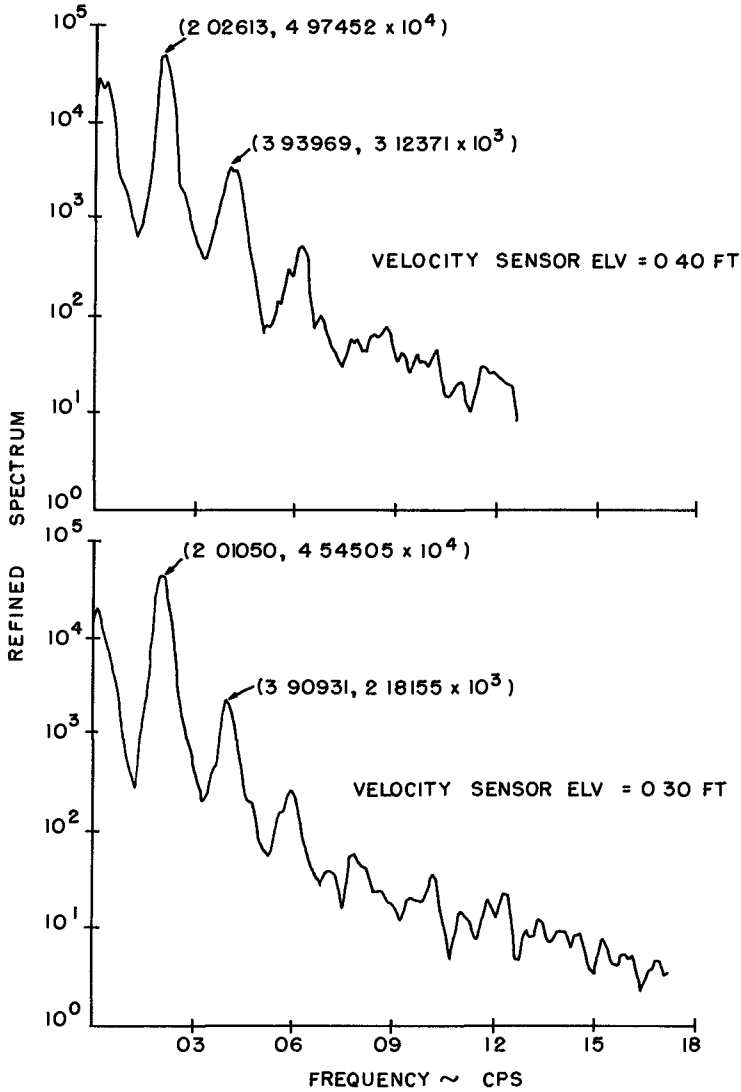


FIG 2C POWER SPECTRAL DENSITY VS FREQUENCY

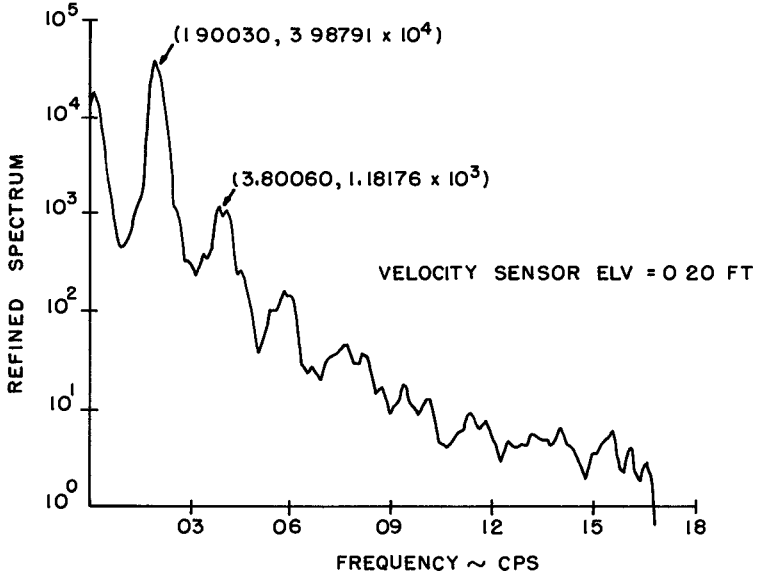


FIG 2D POWER SPECTRAL DENSITY VS FREQUENCY

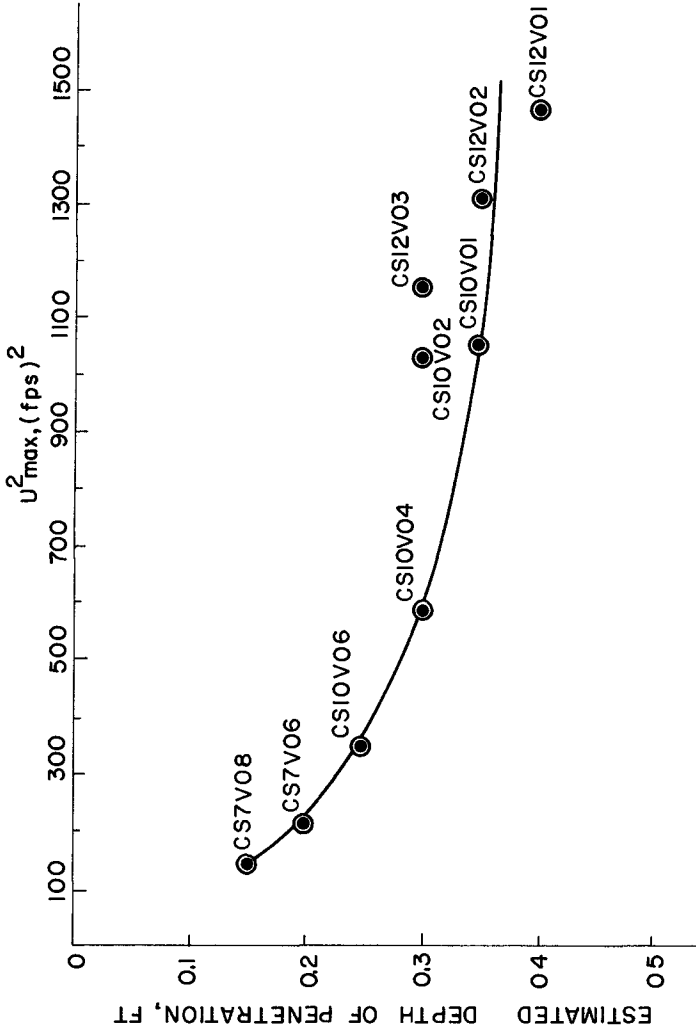


FIG 3 ESTIMATED DEPTH OF PENETRATION OF MACRO - TURBULENCE vs MAXIMUM WIND SPEED

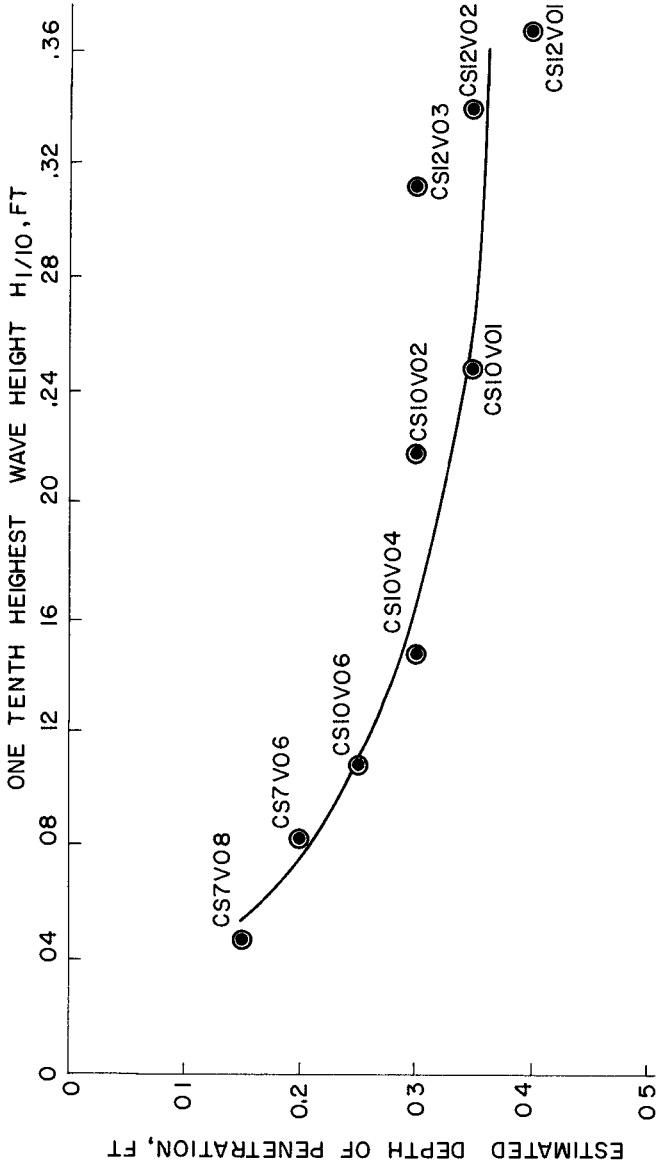


FIG 4 ESTIMATED DEPTH OF PENETRATION OF MACRO - TURBULENCE vs $H_{1/10}$

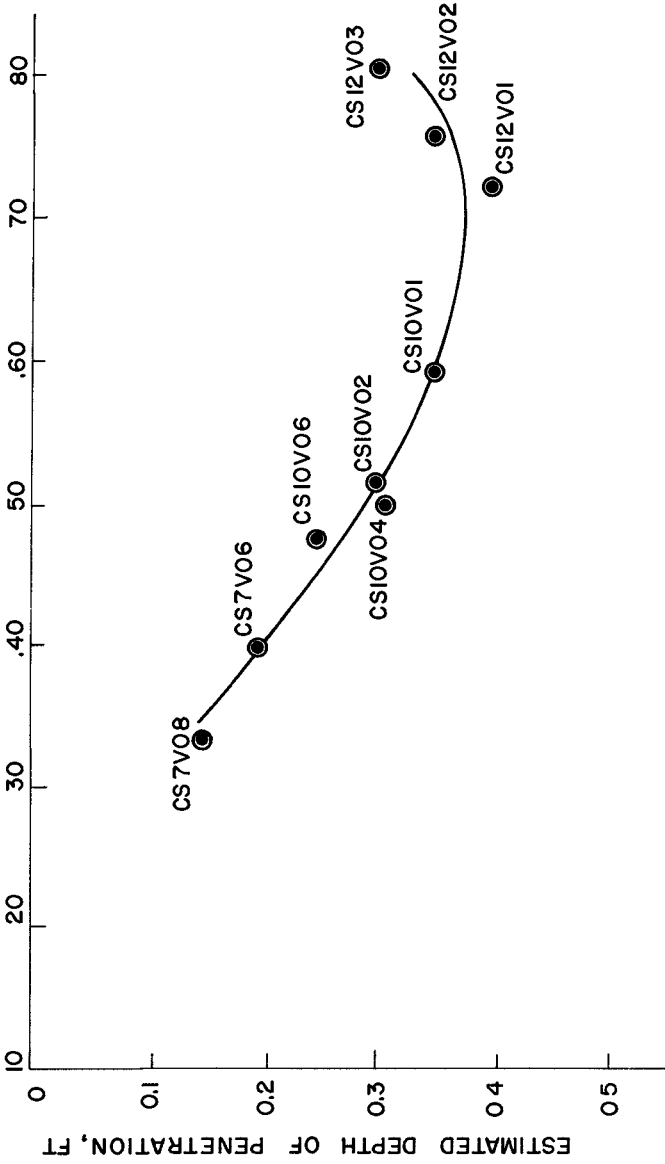


FIG 5 ESTIMATED DEPTH OF PENETRATION OF MACRO-TURBULENCE vs $H_{1/10} / T_{1/10}^2$

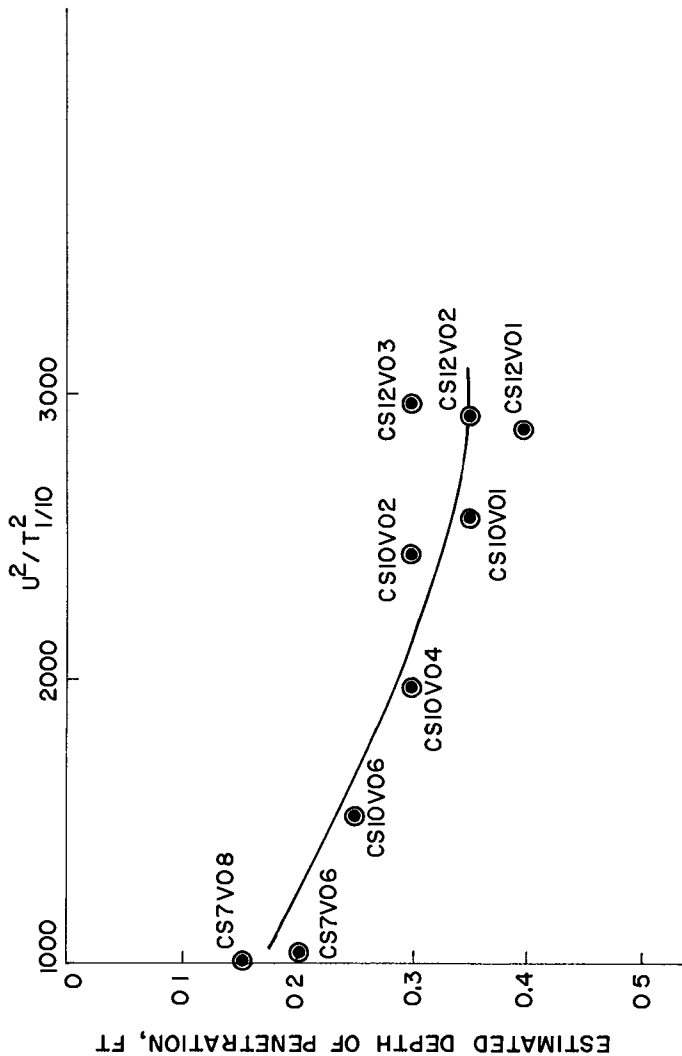


FIG 6 ESTIMATED DEPTH OF PENETRATION OF MACRO-TURBULENCE vs U^2/T^2

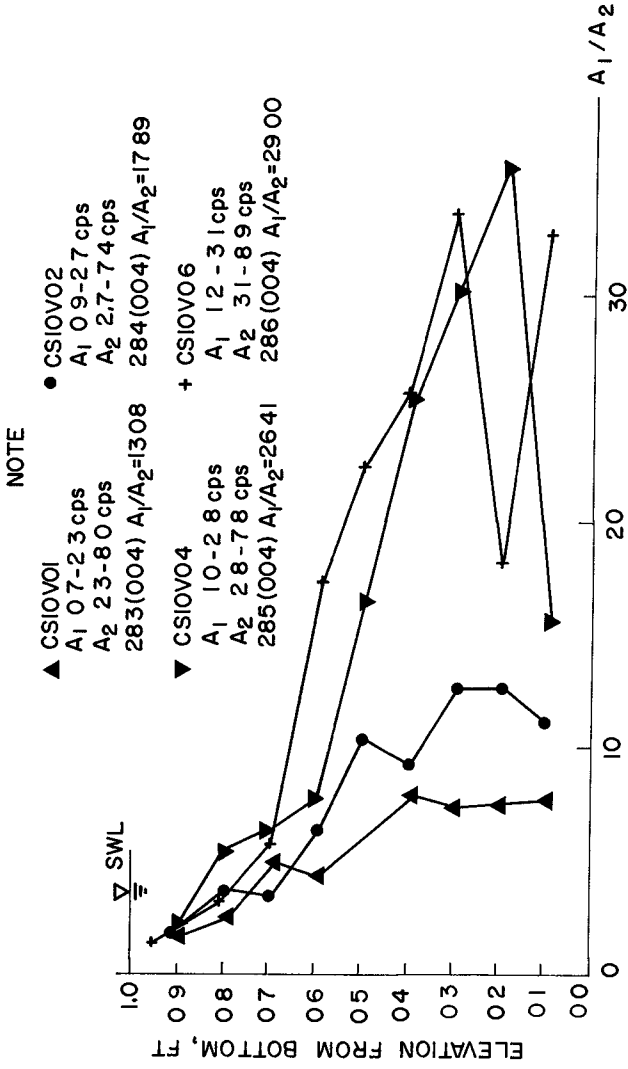


FIG 7 RATIO A₁/A₂, CSIOV01, V02, V04 & V06 SERIES